JOURNAL OF GEOPHYSICAL RESEARCH, VOL. 104, NO. C4, PAGES 7715–7728, APRIL 15, 1999

Estimates of bottom roughness length and bottom shear stress in South San Francisco Bay, California

Ralph T. Cheng, Chi-Hai Ling, and Jeffrey W. Gartner

Water Resources Division, U. S. Geological Survey, Menlo Park, California

P. F. Wang

Marine Environmental Quality Branch, Space and Naval Warfare Systems Center, San Diego, California

Abstract. A field investigation of the hydrodynamics and the resuspension and transport of particulate matter in a bottom boundary layer was carried out in South San Francisco Bay (South Bay), California, during March-April 1995. Using broadband acoustic Doppler current profilers, detailed measurements of turbulent mean velocity distribution within 1.5 m above bed have been obtained. A global method of data analysis was used for estimating bottom roughness length z_o and bottom shear stress (or friction velocities u_*). Field data have been examined by dividing the time series of velocity profiles into 24-hour periods and independently analyzing the velocity profile time series by flooding and ebbing periods. The global method of solution gives consistent properties of bottom roughness length z_o and bottom shear stress values (or friction velocities u_*) in South Bay. Estimated mean values of z_o and u_* for flooding and ebbing cycles are different. The differences in mean z_o and u_* are shown to be caused by tidal current flood-ebb inequality, rather than the flooding or ebbing of tidal currents. The bed shear stress correlates well with a reference velocity; the slope of the correlation defines a drag coefficient. Forty-three days of field data in South Bay show two regimes of z_o (and drag coefficient) as a function of a reference velocity. When the mean velocity is >25-30 cm s^{-1}, the ln z_o (and thus the drag coefficient) is inversely proportional to the reference velocity. The cause for the reduction of roughness length is hypothesized as sediment erosion due to intensifying tidal currents thereby reducing bed roughness. When the mean velocity is <25–30 cm s^{-1}, the correlation between z_o and the reference velocity is less clear. A plausible explanation of scattered values of z_o under this condition may be sediment deposition. Measured sediment data were inadequate to support this hypothesis, but the proposed hypothesis warrants further field investigation.

1. Introduction

The mechanisms that control the transport, erosion, and deposition of fine sediments in tidal estuaries are directly influenced by highly variable hydrodynamic conditions near bed and by sediment bed composition (sediment types and sizes). To determine the hydrodynamic characteristics, direct measurements of velocity in benthic turbulent boundary layer were made using a few (4~6) current meters placed near bed [*Gross and Nowell*, 1983; *Drake and Cacchione*, 1986; *Grant et al.*, 1984; *Grant and Madsen*, 1986]. In estuaries, momentum loss and energy dissipation near the sediment-water interface give rise to high velocity gradients (shear) in the bottom boundary layer (BBL). Since the velocity gradient is large, using 4-6 velocity sensors may not be sufficient to accurately determine the velocity distribution in the BBL for estimates of friction velocity u_* and bottom roughness length z_o [*Grant and Madsen*, 1986]. The shear stress near bed directly causes sediment erosion and affects vertical mixing and conditions conducive to sediment deposition. Furthermore, hydrodynamic properties in the BBL determine relationships among tidal velocity, bottom shear stress (friction velocity), sediment bed roughness, and near-bed sediment response to flows.

To estimate bottom shear stress, detailed and accurate velocity profiles in turbulent bottom boundary layer must be determined. In an exploratory experiment, *Cheng et al.* [1997a] measured near-bed tidal velocity by mounting an acoustic Doppler current profiler (ADCP) on a bottom platform with the acoustic beams pointing vertically down. Velocity distributions within the BBL (1.5 m) were measured by a broadband ADCP (BB-ADCP) operating in a high-resolution mode. Measured time series consisted of velocity profiles determined at 5-cm intervals in the vertical and recorded every 2 min. Although the results from this exploratory experiment were convincing, there were no independent velocity measurements that could be used to validate these ADCP velocity measurements in the BBL.

Following *Cheng et al.* [1997], a series of field investigations were conducted utilizing concurrent deployments of ADCPs and a geoprobe. The geoprobe is an instrumented bottom tripod which was designed specifically for studies of the BBL [*Cacchione and Drake*, 1979]. This paper reports some results of the field investigation in South San Francisco Bay, California, during March-April 1995. The field experiment was quite

Paper number 1998JC900126.

successful; nearly all sensors recorded time series data up to 45 days. Only field data that are related to properties of the BBL are presented and discussed in this paper. A global method for estimating friction velocity u_* (or bottom shear stress) and bottom roughness length z_o is proposed and used. Compared to the conventional method of data analysis, the global method leads to more consistent estimates of roughness length z_o and friction velocity u_* from which correlations among tidal velocity outside of the boundary layer (reference velocity), z_o, drag coefficient, and u_* can be established.

In the following the study site and instruments used in the field experiment will be briefly summarized. A description of the general ambient flow conditions and the velocity measurements in the BBL during the field experiment will be presented. The global method for computing BBL properties and an error analysis of the method will be introduced. The main results from this data set include the estimates of bottom shear stress and roughness length. Deduced BBL properties are shown to be functions of a reference velocity and independent of flooding or ebbing preference. Field data show that z_o (thus the drag coefficient) correlates well with a reference velocity. Hypotheses are proposed suggesting possible mechanisms that support this correlation.

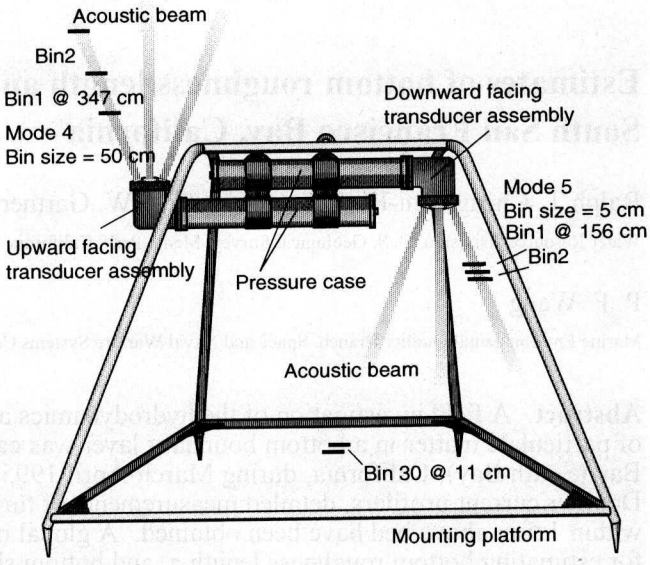

Figure 2. Schematic diagram of the bottom platform supporting the upward and downward pointing broadband acoustic Doppler current profiler (BB-ADCP) pair.

2. Field Site and Experiment

San Francisco Bay is a complex estuarine system comprising two distinct hydrologic sub-estuaries: the northern reach and South San Francisco Bay (South Bay) (Figure 1). The field experiment was carried out in South Bay, which is a semienclosed tidal basin connecting to Central Bay at its northern end. Normally, South Bay is vertically well mixed except during periods of high local runoff and river discharge [*Schoellhamer*, 1996; *Cheng et al.*, 1997]. Tides and tidal currents in the bay are mixed diurnal and semidiurnal types, mainly semidiurnal with distinctive spring-neap variations. In general, the dynamics of the BBL could be affected by many factors such as wind-wave current interactions, influence of stratification, and unsteadiness of tidal flows. The study site was deliberately chosen to have a simple physical setting to delineate hydrodynamic properties from complications due to bathymetry and stratification. The study site was in the main channel of South Bay where the bathymetry near and around the deployment is relatively flat and smooth (Figure 1). The water depth is ~16 m relative to mean lower low water (MLLW). At that depth, surface wind waves at the study site are not expected to penetrate to bottom; thus it is not necessary to consider wave effects in boundary layer analysis. Although furrows have been reported in this region, a side-scan sonar survey identified a smooth area without furrows which was considered to be suitable for instrument deployment. Maximum tidal currents near bed are expected to be in excess of 80 cm s^{-1} and strongly bidirectional [*Cheng et al.*, 1997, 1998]. During the study period, up to 3-4 ppt salinity stratification over the water column has been recorded. For the most part, however, the water column representing the BBL (~2 m) can be assumed to be vertically well mixed. Thus the effects due to salinity stratification are not considered in this analysis. The sediment compositions in the vicinity of the study site are mostly silt and clay-mud whose mean particle size is <62 μm [*Nichols and Thompson*, 1985; *Kranck and Milligan*, 1992]. There are also shell fragments underlying fine sediments at the study site. In shallow areas to the east of the study site, mud is mixed with sand and shell fragments. The deliberate choice of a simple physical setting for the study site limited the primary forcing of the hydrodynamic boundary layer to barotropic tidal current only.

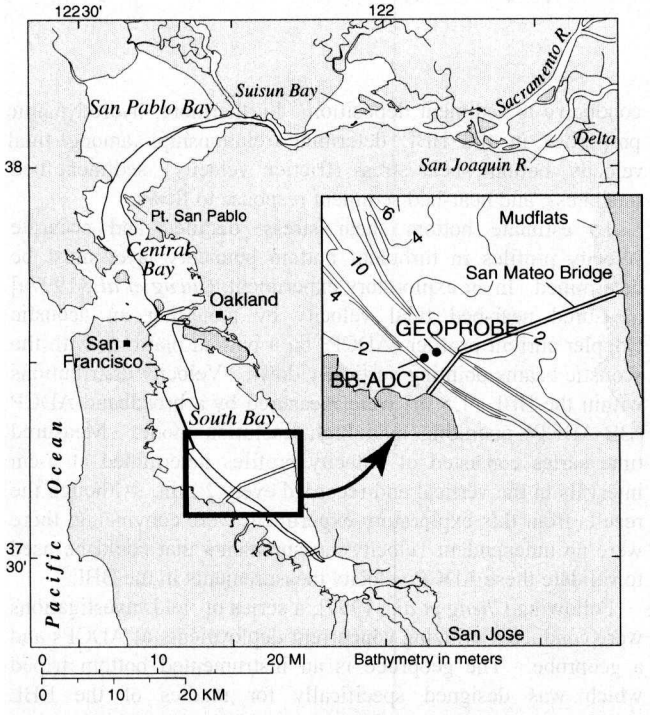

Figure 1. Study site: South San Francisco Bay near San Mateo Bridge where the water depth is ~16 m referenced to mean lower low water (MLLW).

A cluster of in situ recording instruments was deployed in the main channel of South Bay ~1 km north of San Mateo Bridge (Figure 1). Two BB-ADCPs were deployed on the same platform (Figure 2) at ~2 m above bed; one unit was mounted

with the transducers pointing vertically up, and the other was mounted with transducers pointing vertically down. There were two conductivity-temperature-depth (CTD) data loggers and two optical backscatterance sensors (OBS). The pair of 1200 kHz BB-ADCPs measured tidal velocity from near bed to ~2-3 m below free water surface [*Gartner and Cheng*, 1996]. The upward pointing ADCP was operating in mode 4 [*Gordon*, 1996], which recorded tidal current velocity profiles from 3.5 m above bed (center of the first bin) to ~3 m below water surface in 50-cm increments. The downward pointing BB-ADCP was programmed to operate in a high-resolution mode 5 [*Gordon*, 1996], which measured velocities from 1.56 m to an estimated distance of 6 ± 1~2 cm (at bin 31) above bed in 5-cm intervals. The BB-ADCP in high-resolution mode (mode 5) compromises the range of operation to 4 m instead of ~20 m in mode 4. For the present purpose the shortened range of operation was more than sufficient to measure velocity profiles in the BBL. For each velocity measurement, sufficient acoustic pings were sent whose echoes were averaged such that the standard deviation (error) of the recorded velocities was estimated to be <0.7 cm s^{-1}. The upward pointing ADCP recorded mean velocity profiles at 10-min intervals whereas the downward pointing BB-ADCP measured turbulent boundary layer velocity profiles every 2 min.

A geoprobe was deployed within ~50 m from the ADCP platform. The geoprobe bottom tripod has been used extensively in studies of BBL on continental shelves [*Cacchione et al.*, 1995]. The sensors on the geoprobe include four electromagnetic (EM) current meters, OBS sensors, infrared light emitting diode (LED) Transmissometers, a CTD, and a recording fluorometer for measurements of chlorophyll a concentration. The four EM current meters were mounted at estimated heights of 19, 52.5, 86.5, and 120 cm above bed. The EM current meters on the geoprobe were set to record a burst of 1024 instantaneous velocity readings at 1 Hz every 60 min. The accuracy of the EM current meters specified by the manufacturer is ±0.5 cm s^{-1}. After suitable temporal averages, turbulent mean flows determined by the EM current meters were compared with concurrent ADCP measurements [*Gartner and Cheng*, 1996].

3. Results

Nearly all sensors recorded time series data covering the entire deployment period from February 28, 1995, to April 11, 1995. The tides in the bay have pronounced spring-neap tidal variations. Tidal amplitudes at spring tides can be twice as much as those at neap tides. Distinctive spring-neap tidal variations in San Francisco Bay suggest that all related hydrodynamic, sedimental, biochemical, and particulate transport properties are potentially varying in a spring-neap cycle [*Walters et al.*, 1985]. Measured water level variations show a typical spring-neap tidal cycle. The tidal range is ~1.5 m during neap tide and 2.5 m during spring tide (Figure 3a). The time series of tidal current measured at 156 cm above bed, U_{156}, is plotted in direction and speed versus time (Figures 3b and 3c). The tidal current speed varies in spring-neap cycles in concert with variations of sea level. In this deployment the tidal current varies from weak ebb-dominant flows (days 60-72), to strongly ebb-dominant flows (days 77-85), to no dominance in ebb or flood (days 85-95), and to weak flood dominant flows (days 95-102). These tidal current ebb-flood properties, which may play an important role in defining some boundary layer properties, will be further discussed in later sections. An unusual flow event took place between days 67 and 70 when a major storm moved through northern California. The time series of wind direction and speed are shown in Figures 3d and 3e. Discussions of this unusual flow event were given by *Cheng et al.* [1998] and will not be repeated here.

3.1. Velocity Measurements in the Boundary Layer

Before utilizing the detailed velocity measurements for characterizing sediment bed and hydrodynamic properties it is necessary to ascertain that these velocity measurements made by a BB-ADCP were indeed valid and accurate. If validated, high-resolution turbulent mean velocity profiles can then be used to estimate bottom shear stress (friction velocity u_*) and bottom roughness length z_o and can be used to evaluate bottom boundary layer theories.

The downward pointing BB-ADCP was mounted on a platform at a distance of ~2 m above bed (Figure 2). This setup is essentially the same as a boat-mounted ADCP in discharge measurement, except the boat is stationary. In mode 5 the BB-ADCP uses pulse-to-pulse coherence principle for signal processing [*Lohrmann et al.*, 1990; *Lhermitte and Lemmin*, 1994]. Unfortunately, these double-pulsed signals can decorrelate when the water speed exceeds ~45-50 cm s^{-1} or when turbulence is too intense. The decorrelation of signals is due to the long time lag between pulses in mode 5 rendering the velocity measurements invalid. In this deployment the original 2-min time series of mean velocity profiles in the BBL was obtained from averaging up to 20 single ping velocity measurements. When the correlation coefficient is lower than a predetermined threshold (R^2 <0.25), that single ping measurement is decorrelated and excluded from the mean profile calculation. In practice the recorded correlation coefficients are generally either >0.75 or zero (completely decorrelated). In the latter case the measurements are decorrelated and dropped out. The instrument also recorded the percentage of good data ("percent good"). When the percent good is <25%, the mean profile is considered invalid because the standard deviation for the mean flow measurement becomes too high. When the mean velocity approaches ~40-50 cm s^{-1}, some single ping measurements drop out because of decorrelation. The net effect is that the mean velocity profile is determined by fewer single ping measurements, leading to a slightly higher standard deviation. Since decorrelation occurs when the velocity is high the mean velocity near the threshold velocity is biased to a slightly lower value. During data analysis a 10-min time series of velocity profiles was constructed from the 2-min time-series. Therefore a 10-min averaged velocity profile is the ensemble average of up to 100 single ping measurements. The percentage of good profiles is nearly 100% when the mean velocity is low. As the mean velocity approaches the threshold of decorrelation, the percentage of good data decreases sharply. The net effect is an increase in standard deviation and an introduction of a bias error leading to underestimating the mean velocity. This bias error in the 10-min velocity time series, of the order of 1-2 cm s^{-1} might affect the results of boundary layer analysis. The errors in the BBL properties due to this bias error will be examined and discussed further in later sections.

Although the ADCP setup parameters were chosen to minimize data loss due to decorrelation, ~25% of time series data were lost because of low signal correlation in periods of high tidal speed (especially during maximum ebb). Despite this limitation the use of BB-ADCP for high-resolution velocity

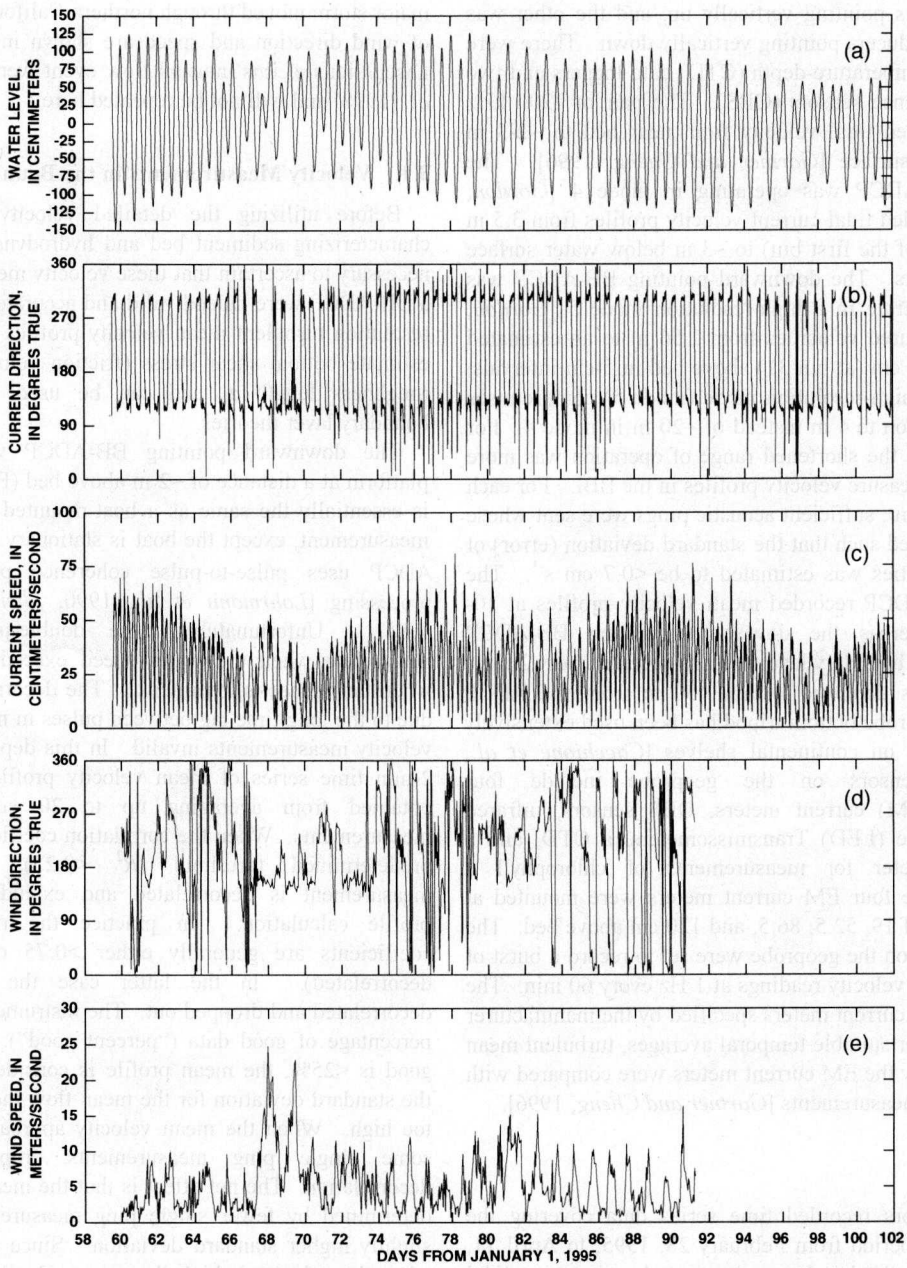

Figure 3. Time-series of (a) tides, (b) tidal current direction, (c) tidal current speed at 156 cm above bed, U_{156}, (d) wind direction, and (e) wind speed between February 28 (day 59) and April 14 (day 97), 1995.

measurement is unique. The velocity profiles are collected starting at a distance ~40 cm away from the transducers (blanking distance) in 5-cm intervals. In this experiment, there are 31 bins of "good" data in which the center of bin 31 is estimated to be at ~6 ± 1~2 cm above bed. Small uncertainties regarding the vertical positions of bins remain that are caused by sinking the instrument platform into sediment bed initially at deployment. The amount of sinking cannot be determined precisely. However, analysis of velocity data show, other than the initial sinking of the platform, that there is no evidence of further sinking of the platform throughout the deployment period. The velocities measured at bin 31 (6 cm above) appear to be only partially valid. Some measurements are consistent with velocities at bin 30 or bin 29, but at times the measured velocities are obviously invalid. Thus the time series data at bin 31 are not used in the analysis.

To validate the velocity measurements in the BBL, several independent approaches are used. The velocities measured at bin 1 (3.5 m above bed) from the upward pointing BB-ADCP are compared with velocities measured at bin 1 (1.56 m above bed) from the downward oriented BB-ADCP operating in high-resolution mode (Figure 4a). The correlation between these data sets shows that the velocities at 3.5 m is on average 16% higher than the velocities at 1.56 m. The linear correlation gives a goodness of fit, R^2, of ~0.94. More directly, the measured speeds by the EM current meters on geoprobe at 87 and 53 cm above bed are compared with velocities measured at respective heights by the downward oriented, high-resolution BB-ADCP

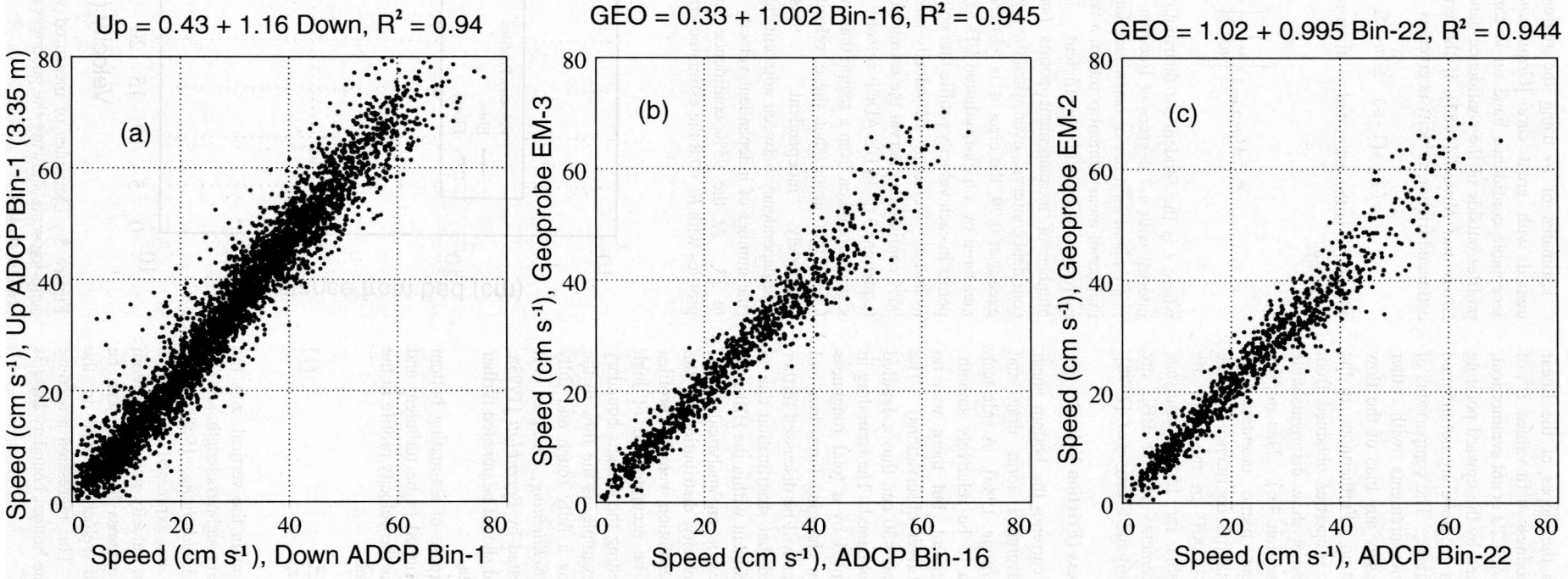

Figure 4. (a) Comparison of bin 1 upward pointing and bin 1 downward pointing ADCP data. (b) Comparisons of downward pointing ADCP data at bin 16. (c) At bin 22 with velocity measurements obtained by electromagnetic current meters on the geoprobe.

(Figure 4b and 4c). In both cases the slopes of the linear correlation are nearly 1.0 with the goodness of fit values, R^2, of ~0.94. The frame for supporting the ADCPs is not symmetrical, but the velocity measurements obtained by the upward pointing ADCP and the EM current meters on geoprobe are not affected by the orientation of the instrument frame. The comparisons of the downward pointing ADCP measurements with other independent measurements did not show any bias of the flow due to the instrument frame orientation. Furthermore, in the present analysis the boundary layer properties obtained from sub-data sets of floods and ebbs did not show distinguishable differences in their properties (see section 3.6). This implies that any effect due to instrument frame orientation is insignificant. These comparisons establish confidence that the velocity profiles measured by BB-ADCP in the BBL are sufficiently accurate and are suitable for further analysis. Further details of velocity measurements in the BBL are discussed by *Gartner and Cheng* [1996] and *Cheng et al.* [1998].

3.2. Estimate of Bottom Shear Stress (Friction Velocity, u_*)

In the absence of wave-induced currents the bottom shear stress is the sum of an areal-averaged form drag and hydrodynamic drag [*Drake and Cacchione*, 1986]. A side-scan sonar survey showed the study area to be relatively smooth. Some furrows might have been present, but there was no evidence of significant bed forms (diver observations). The near-bed visibility at the study site was <30 cm; thus a detailed description of bed form could not be obtained. The form drag in the BBL is assumed to be represented by a total roughness length. Possible correlation between changing form drag and the velocity outside the boundary layer will be discussed further in a later section. It is also assumed that stratification due to water density or due to suspended sediment within the BBL was insignificant. Yet to be determined is an analytical model representing the turbulent mean velocity distribution in the boundary layer. Since the high-resolution velocity profiles measured by BB-ADCP appear to be accurate and of high quality these data are suitable for testing the various boundary layer models and hypotheses. For example, is the flow in the BBL obeying the law of the wall as a fully rough and fully developed turbulent boundary layer [*Schlichting*, 1962], or is it behaving like a power law as suggested by *Barenblatt* [1993a, b]? These issues are fundamental and should be pursued further using high-quality velocity profile data.

As an initial attempt, for the purpose of estimating bottom shear stress, flow in the BBL is assumed to be turbulent and fully rough. Under these assumptions the velocity profile in the BBL is described by the law of the wall,

$$u(z) = \frac{u_*}{\kappa} \ln \frac{z}{z_o} \tag{1}$$

where $u(z)$ is the velocity distribution in the vertical, z is the distance from the bed, z_o is the bottom roughness length, and κ = 0.41 is the von Karman constant [*Schlichting*, 1962]. The apparent bottom shear stress can be expressed in friction velocity as $\tau_b/\rho = (u_*)^2$. The friction velocity u_* or the bottom shear stress τ_b, and the bottom roughness length z_o, can be estimated by fitting the measured velocity profile to the logarithmic velocity distribution (1). This regression procedure implicitly assumes that the flow in the bottom boundary layer is self-similar, and independent of time.

Estimates of u_* using the regression procedure must be treated with great care [*Grant and Madsen*, 1986]. An acceptable confidence band on u_* can be chosen, and velocity profiles outside of the confidence band are rejected. Following *Gross and Nowell* [1983], if the error in u_* is ϵ, then the estimated friction velocity is given as

$$(\tilde{u}_*)(1-\epsilon) \le u_* \le (\tilde{u}_*)(1+\epsilon) \tag{2}$$

where $\tilde{u}_*$ is the estimated u_* from regression. The error ϵ is given by

$$\epsilon = (t_{\alpha/2,n-2}) \left[\frac{1}{n-2} \left(\frac{1-R^2}{R^2} \right) \right]^{1/2} \tag{3}$$

where t is the Student's t distribution for (1 - α) confidence interval with n-2 degrees of freedom. The errors for estimated z_o are about an order of magnitude larger than ϵ. Here n is the number of measurement points in a velocity profile, and R is the regression correlation coefficient. If there are only a small number of measurement points (say, n = 4) at the 95% confidence interval, even when the regression coefficient R^2 is in excess of 0.99, the error ϵ is >±40%. Using the velocity data measured by a high-resolution BB-ADCP, there are 30 velocity points in each velocity profile that could be used for estimates of u_* and z_o. Rejecting all velocity profiles with R^2 <0.8, at the 95% confidence interval the estimated errors for u_* are <±19%, (equation (3)). In BB-ADCP velocity measurements the acoustic signals are taken from a region that overlaps with adjacent bins. One might argue that these velocity measurements are not completely "independent." Assuming there is 25% interdependency between adjacent bins, the degree of freedom (the number of independent velocity measurements) is reduced to 23. At the 95% confidence level, by rejecting velocity profiles with R^2 <0.8 the estimated errors are <±22%. Therefore

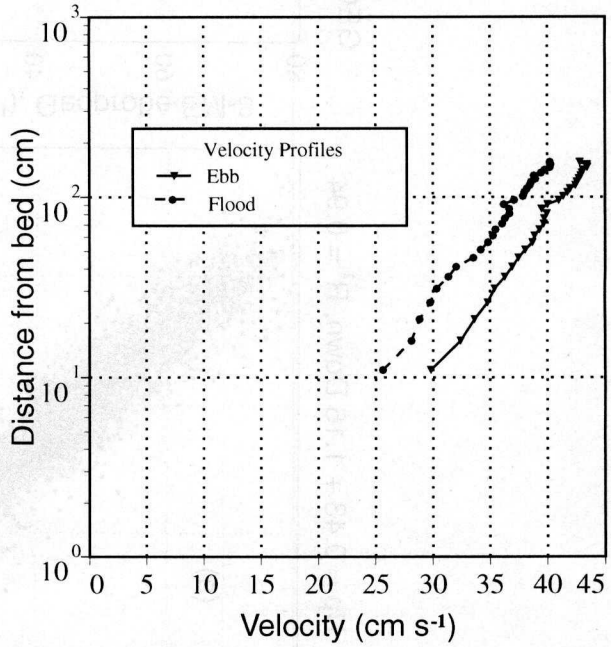

Figure 5. Examples of measured velocity profiles plotted in semi-log scale showing the goodness of fit to the law of the wall (equation (1)).

the present experimental setup is still far superior than measuring velocity profiles by a few (4-6) current meters. In the entire time series (~43 days), 62% of the velocity profiles met the 95% confidence interval with the estimated relative error for u_* <22% ($R^2 < 0.8$).

As discussed in previous sections, when the mean velocity is near the threshold velocity for decorrelation, the velocity measured by a BB-ADCP in mode 5, $U(z)$, underestimates the true velocity $u(z)$, with a bias error $\Delta \geq 0$. When the measured velocity is used in the analysis, the estimated roughness length z_o' is given by

$$U(z) = \frac{u_*}{\kappa} \ln \frac{z}{z_o'} \tag{4}$$

The bias error is related to z_o in (1) and z_o' as

$$\Delta = u(z) - U(z) = \frac{u_*}{\kappa} \ln \frac{z_o'}{z_o} \geq 0$$

or

$$z_o = z_o' \exp(-\Delta\kappa/u_*) . \tag{5}$$

Since Δ, κ, and u_* are positive, $(-\Delta\kappa/u_*)$ is of the order of -0.2. Thus the estimated roughness length z_o' has a factor of up to 20% higher than the roughness length without bias error. Because the possible bias error in roughness length is relatively minor, it will not be distinguished in further discussions.

There are many reasons for rejecting a velocity profile. For example, during periods of acceleration and deceleration the velocity profiles may not be logarithmic. In the initial screening these profiles were eliminated. There could be erroneous measurements due to hardware limitations. In this time series data most rejected velocity profiles were caused by decorrelation of double-pulsed acoustic signals. Following the conventional approach for data analysis, the mean values of u_* and z_o are found to be 1.76 cm s^{-1} and 0.619 cm, respectively. Even in conventional approach, the statistical errors are reduced when more velocity data points are available. Two examples of measured velocity profiles, plotted in semilog scales, are shown in Figure 5. While the mean value of u_* seems to be consistent with previously reported values by *Sternberg et al.* [1986] and *Cheng et al.* [1997a]; however, very few discussions of z_o in San Francisco Bay are available. The computed z_o shows values scattered by as much as a few orders of magnitude, and the arithmetic mean value of z_o seems to be unreasonably high.

3.3. Estimate of Bottom Roughness Length, z_o

The total bed roughness element, k_b, is a complicated function of grain size at the water-sediment interface, hydrodynamic form drag due to bed forms, and sediment transport near the bed. The total bed roughness element k_b can be expressed as

$$k_b = k_{\text{grain}} + k_{\text{drag}} + k_{\text{sediment}} \tag{6}$$

where k_{grain} is grain roughness element due to the physical grain composition of the bed, k_{drag} is the hydrodynamic form drag, and k_{sediment} is due to sediment movements, [*Xu and Wright*, 1995]. In idealized fully rough turbulent boundary layer the total roughness element can be approximated by $k_b \approx 30 z_o$, [*Yalin*, 1977]. The roughness values due to form drag and due to sediment movements are seldom known precisely. Assuming, for the moment, that both the form drag and the sediment movement roughness are insignificant, then the roughness length z_o should be a physical quantity that remains fixed when the characteristics of sediment bed remain unchanged. On the basis of this observation, *Ling and Untersteiner* [1974] proposed a method for deducing u_* and z_o from the steady state air boundary layer over sea ice. The proposed method assumes that z_o remains constant and is solved along with several u_* values. As documented by *Ling* [1976], the method produces consistent value of roughness length z_o and greatly reduces scattering in friction velocities u_* using air boundary layer data over a flat plate and compared with direct measurements of drag and bottom shear stress in Kansas [*Izumi*, 1971].

In this paper this approach is adapted and extended to analyze properties of unsteady BBL flows in tidal estuaries. On the basis of the argument of physical characteristics of the flow, z_o is assumed to remain fixed for a period of time (several hours in this case) in which N velocity profiles are measured. Instead of fitting each velocity profile for a pair of u_* and z_o, N velocity profiles are fitted simultaneously to the law of the wall for N values of u_* and one z_o characterizing the bed roughness spanning the interval covered by the data set. Hereinafter this method of analysis is referred to as the "global method" implying that the analysis ties all N velocity profiles in one step of regression. The global method is based on the physical argument that there exists a mean value of the roughness length for the time interval; therefore the choice of a subtime period in which the assumption is valid is somewhat subjective. Furthermore, this approach may work well in some cases but may not apply in others depending upon the properties of sediment bed. A more definitive statement can only be made after the method has been tested in several distinctively different situations.

The global method is used to describe the sediment bed characteristics in this study. Accordingly, the bed roughness is assumed to remain unchanged for 5 - 25 hours. The time series of high-resolution velocity profiles collected in the BBL are sorted into sub-data sets with each sub-data set representing either a day, an ebbing period, or a flooding period. Within each subperiod a mean bed roughness length exists and is assumed to be constant. Between subperiods the mean bed roughness length changes in response to changing flow conditions outside of the boundary layer. The choice of a sub-data set is a judgement of the user; the physical significance of the deduced boundary layer properties should be interpreted accordingly.

Each velocity profile contains 30 measurement points at 5-cm intervals (data at bin 31 are not used). The closest velocity measurement is estimated to be at ~11 ± 2 cm above bed. In the boundary layer analysis the original 2-min interval time series is time-averaged to produce a 10-min time series, giving a maximum of 144 profiles per day. Before the global method is applied the velocity time series data are processed by the conventional method. The erroneous data due to decorrelation of acoustic signals, nonlogarithmic velocity profiles due to acceleration, or deceleration of flow during slack tides are screened and rejected if the velocity profile has R^2 <0.8. The resulting daily time series contain between 33 and 100 usable "logarithmic" profiles in a typical data subset. Starting from February 28, 1995, each daily velocity profile subset is analyzed by the global method to obtain a daily mean value of roughness length z_o and estimates of u_* values for each qualified velocity profiles within that day. These calculations give a total of 43

daily values of $z_{o_{global}}$. The arithmetic mean daily values of $z_{o_{conv}}$ obtained by the conventional method are computed and compared with daily values of $z_{o_{global}}$. Although the trends in daily values of $z_{o_{global}}$ and $z_{o_{conv}}$ are similar, $z_{o_{conv}}$ is an order of magnitude greater than $z_{o_{global}}$ as shown in Figure 6. The global method gives a mean $z_{o_{global}}$ value of ~0.134 cm or ~4 cm for the total roughness element k_b. The values of $z_{o_{global}}$ are quite reasonable on the basis of reports and observation of the bottom surface conditions by diver. On the other hand the arithmetic mean of conventional $z_{o_{conv}}$ is ~0.62 cm or equivalent to a total roughness element for the bed to be ~20 cm. This estimate appears to be too high.

In the conventional method of solution each measured velocity profile is fitted to a straight line on a semilogarithmic scale. The vertical intercept, ln z_o, determines $z_{o_{conv}}$. Therefore a proper estimate of mean z_o values should be defined as

$$z_{o_{log}} = \exp< \ln(z_{o_{conv}}) > \tag{7}$$

where < > represents an arithmetic average. Equation (7) suggests that the mean z_o is given by the inverse function of mean intercepts on a semilogarithmic scale or mean value of ln $z_{o_{conv}}$. The third curve in Figure 6 is the daily values of z_o computed by (7). As shown in Figure 6, the $z_{o_{log}}$ defined by mean intercepts differs little from $z_{o_{global}}$. This method is hereafter referred to as the log-averaged method. The present data set shows that the log-averaged method is a good approximation for the global method in defining z_o. The log-averaged method is simple and might be quite useful. The close agreement between the mean daily values of $z_{o_{log}}$ and $z_{o_{global}}$ is quite significant. No further assumptions are introduced in the log-averaged method; only the computation of the mean z_o value is based on the mean value of ln $z_{o_{conv}}$. The close agreement between $z_{o_{log}}$ and $z_{o_{global}}$ supports the assumption that z_o can be treated as a constant for the subperiod in the global method. This agreement also suggests that the log-averaged method can be used as a simpler and more accurate method than the conventional scheme for estimating mean z_o values. After the initial processing of the velocity profiles by the conventional method a mean z_o for a subperiod can be evaluated by the log-averaged method. Using the fixed z_o, more accurate u_* values can be recomputed using simple regression for a subperiod.

3.4. Error Analysis for Computing Drag Coefficient

Errors exist in field measurements for many reasons. When measured data are used to deduce other physical parameters such as u_* and z_o, these errors are transferred into errors of new variables. The measurement errors could be either controlled or magnified in the final physical variables depending upon the method of analysis. Let $u(z,t)$ denote the exact velocity profile such that the measured velocity profile $U(z,t)$ is

$$U(z,t) = u(z,t) + \varepsilon(z,t) \tag{8a}$$

where $\varepsilon(z,t)$ is the error in measurements (the random measurement error, not bias error). In the initial phase of data analysis the field data are first screened, rejecting nonlogarithmic velocity profiles with R^2 <0.8. At the 95% confidence interval the estimated error is <±22% (equation (3)). Therefore, for the remaining qualified velocity profiles, ε can be assumed to be of higher order when compared to u. Similarly, let (u_*, U_*) and (z_o, Z_o) denote the exact and approximate values of friction velocity and roughness length, so that

$$U_* = u_* + \delta \qquad Z_o = z_o + \zeta \tag{8b}$$

where δ and ζ are errors of u_* and z_o, respectively.

3.4.1. Conventional Method When fitting measured data to the law of the wall using the conventional method of solution, (1) becomes

$$u + \varepsilon = \frac{u* + \delta}{k} \ln \frac{z}{z_O + \varsigma} \tag{9}$$

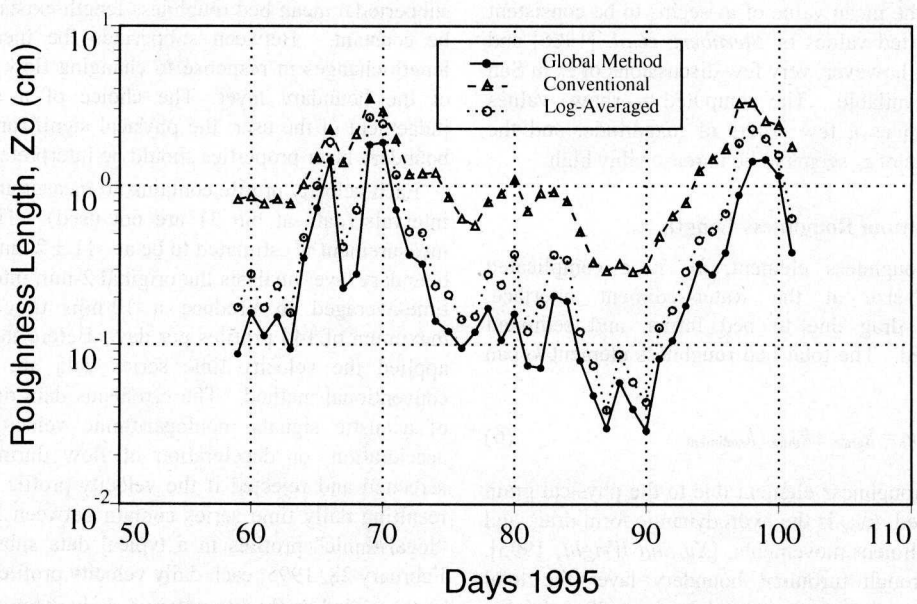

Figure 6. Variations of daily mean roughness length z_o computed by the global method (solid circles), the conventional method (open triangles), and the log-averaged method (open circles).

Equation (9) can be rearranged to read

$$\frac{\delta}{u*} = \frac{\ln\left(1+\frac{\varsigma}{z_O}\right)}{\ln\frac{z}{z_O+\varsigma}} + \frac{\varepsilon}{u*}\left(\frac{k}{\ln\frac{z}{z_O+\varsigma}}\right) \tag{10}$$

Because ζ varies by a few orders of magnitude, both the numerator and the denominator of the first term on the right-hand side of (10) are of the order 1. The second term on the right-hand side is of the order of ε and thus can be neglected when compared with the first term. Therefore (10) implies that the relative error in friction velocity, δ/u_*, is also of order 1 or that the errors in u_* are of the same order of magnitude as u_* itself.

The bottom shear stress τ_b is proportional to friction velocity squared and is also proportional to a reference velocity squared (velocity measured at a reference point above bed). The proportionality constant is defined as the drag coefficient. Assuming the velocity U_{156} at 156 cm above bed (bin 1 in this measurement) is the reference velocity, τ_b can be given as

$$\tau_b / \rho = u_*^2 = C_d (U_{156})^2 \tag{11}$$

Then the drag coefficient C_d is the slope of correlation between u_*^2 and U_{156}^2,

$$C_d = \frac{U_*^2}{U_{156}^2} = \frac{(u_* + \delta)^2}{U_{156}^2} \approx \frac{u_*^2}{U_{156}^2} + 2\frac{\delta u_*}{U_{156}^2}$$

$$= \frac{u_*^2}{U_{156}^2}\left(1 + 2\frac{\delta}{u_*}\right) \tag{12}$$

where the variables in (12) are given in the sense of a correlation. The drag coefficient is shown to vary by as much as $2\delta/u_*$, i.e., of the order 1.

3.4.2. Global Method. Using the same notations defined above for the global method, the law of the wall, (1), is applied to N velocity profiles simultaneously:

$$u_i + \varepsilon_i = \frac{(u_*)_i + \delta_i}{\kappa}\ln\frac{z}{z_o+\varsigma_i} \qquad i = 1,2,...N \tag{13}$$

where the subscript i indicates the ith velocity profile in the data subset. Since the basic assumption in the global method of solution is that the variations in z_o are small, the following expansion holds true:

$$\ln\frac{z}{z_O+\varsigma_i} = \ln\left[\frac{z}{z_o}\left(1-\frac{\varsigma_i}{z_o}+...\right)\right] \approx \ln\frac{z}{z_o} \tag{14}$$

Using (14), (13) becomes

$$u_i + \varepsilon_i = \frac{(u_*)_i + \delta_i}{\kappa}\ln\frac{z}{z_o} \qquad i = 1,2,...N \tag{15}$$

While u_i, u_{*i}, and z_o satisfy (1) exactly, (15) becomes

$$\varepsilon_i = \frac{\delta_i}{\kappa}\ln\frac{z}{z_o} \qquad i = 1,2,...N \tag{16}$$

Dividing (16) by (1), it gives the relative error for friction velocity,

$$\delta_i / u_{*i} = \varepsilon_i / u_i. \tag{17}$$

Thus, the relative error in friction velocities is of the same order as measurement error ε/u, which has been assumed to be of higher order. In the global method of solution the drag coefficient, C_d or the slope of correlation between u_*^2 and U_{156}^2, can be written as

$$C_d = \frac{U_*^2}{U_{156}^2} = \frac{(u_* + \delta)^2}{U_{156}^2} \approx \frac{u_*^2}{U_{156}^2}(1+2\frac{\delta}{u_*}) \tag{18}$$

where δ/u_* is the relative error in friction velocity. Therefore the error in C_d derived in the global method is of higher order. This conclusion can be substantiated by the results derived from the present data set to be discussed in the next section.

3.5. Properties of Bottom Shear Stress, τ_b

As discussed above, the drag coefficient is the slope of the correlation between friction velocity squared and a reference velocity squared. In a statistical sense the drag coefficient can be written as

$$C_d = [u_* / U_{156}]^2 \tag{19a}$$

where U_{156} is the velocity at z =156 cm above bed or z_{156}. When the u_* values are obtained by the conventional method, the correlation between u_*^2 and U_{156}^2 is weak in which the R^2 values were in the range of 0.25-0.8 [*Cheng et al.*, 1997]. In this case the drag coefficient derived by the conventional method is poorly defined. Within the context of the law of the wall the drag coefficient can be written as

$$C_d = [\kappa / \ln(z_{156}/z_o)]^2 \tag{19b}$$

From (19b) it is clear that for the global method the assumption of constant z_o within a short period implicitly implies that a constant drag coefficient exists that can be used to define the bottom shear stress equation (11). For example, the computed u_*^2 for two different days are well correlated with U_{156}^2 as shown in Figure 7. The goodness of fit, R^2, for both days is 0.99. This property is not surprising and is supportive and consistent with the basic assumption of the global method of analysis. It is interesting to point out that the daily mean values of the drag coefficient derived by the global method, over 43 days, vary with the spring-neap tidal cycle (Figure 8). The well-behaved correlation between u_*^2 and U_{156}^2 implies that the global method of analysis also reduces the random errors in u_*. The drag coefficient is well defined within a subperiod, but the drag coefficient varies from subperiod to subperiod. The general trend is that the drag coefficient has a higher value during less energetic neap tides and has a lower value during more energetic spring tides. Similarly, when mean tidal velocity has higher energy (spring tides), the roughness length has lower values. During neap tides, tidal energies are reduced, the roughness length increases to higher values (Figure 6). These properties are quite intriguing; similar roughness length variations have been reported by *Schauer* [1987] on the basis of observations at two shallow coastal sites.

3.6. Effects of Flooding and Ebbing

The bed roughness in the turbulent boundary layer characterizes local turbulence intensity, which is the combination of the turbulence advected from upstream and the local turbulence production. Because the field experimental

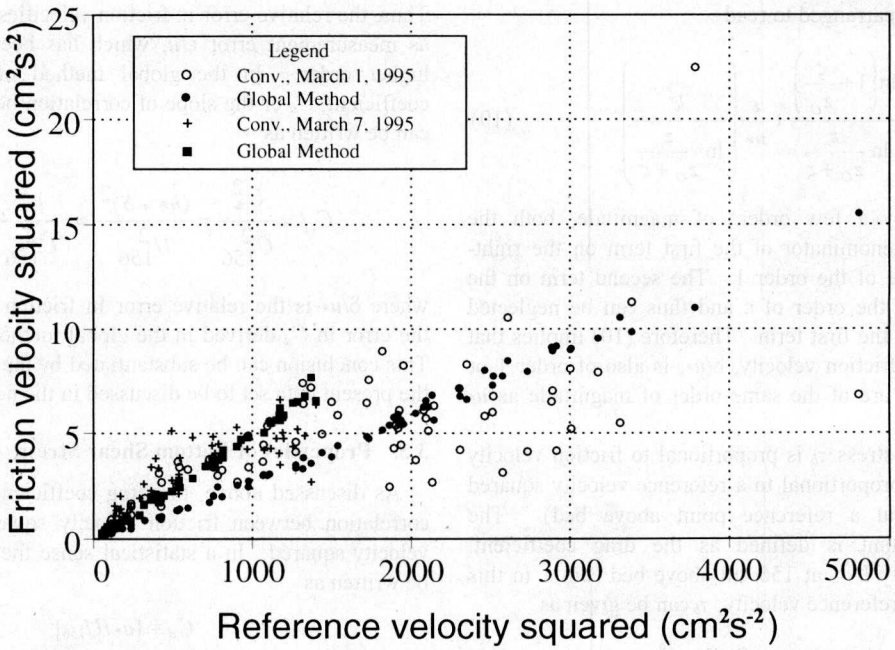

Figure 7. Examples of correlation between bottom shear stress and reference velocity squared: March 1, 1995 (open solid circles), and March 7, 1995 (crosses and solid squares). The R^2 values for a linear fit are 0.99 for the two examples if u_* values were derived by the global method. The R^2 values are 0.25 and 0.80 for March 1 and 7, 1995, respectively, if u_* values were obtained by the conventional method.

setup is rarely symmetric to flooding and ebbing of tidal currents, many researchers choose to analyze field data by separating the time series into flooding and ebbing subsets. Presumably, the nonlocal boundary layer properties for ebbing and flooding cycles might be identified and examined independently. Following this logic, the global method is used to analyze the velocity profiles by dividing the time series into ebbing and flooding cycle subsets. For each ebbing and flooding cycle a single z_o value and a time series of u_* were computed. The resulting z_o values for ebbs (dots) and for floods (crosses) are shown in Figure 9a. The roughness length varies with the spring-neap tidal cycles, but there is not a decisive pattern differentiating the time series of z_o from flooding or ebbing periods. Although the mean value of z_o is lower for ebbing cycles (0.080 cm) than for flooding cycles (0.102 cm), it is premature to conclude that there are different turbulence properties at the study site during ebbing and flooding cycles. Similarly, the mean current speeds for ebbing (dots) and for

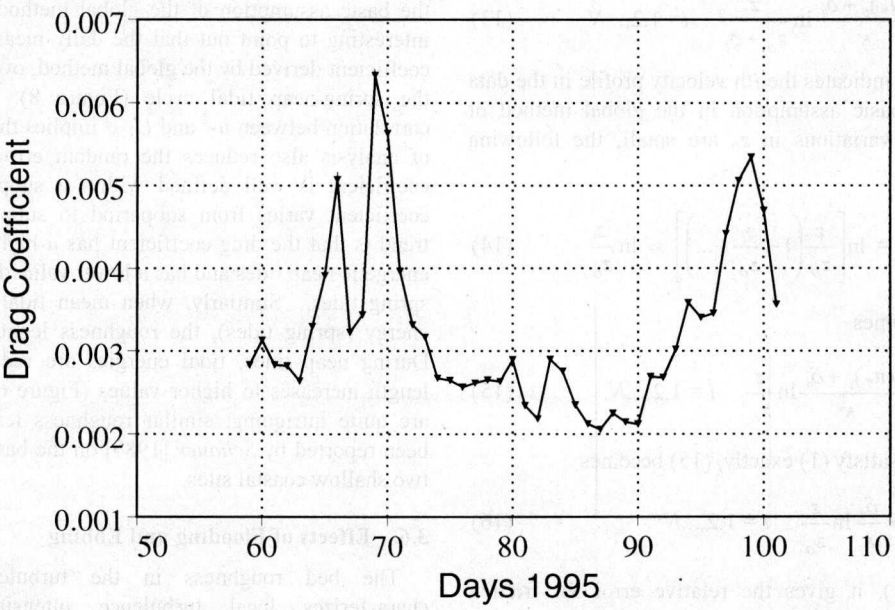

Figure 8. Variations of the daily averaged drag coefficient in spring-neap cycles as computed by the global method. The low values of drag coefficient at days 67 and 68 were during the storm event.

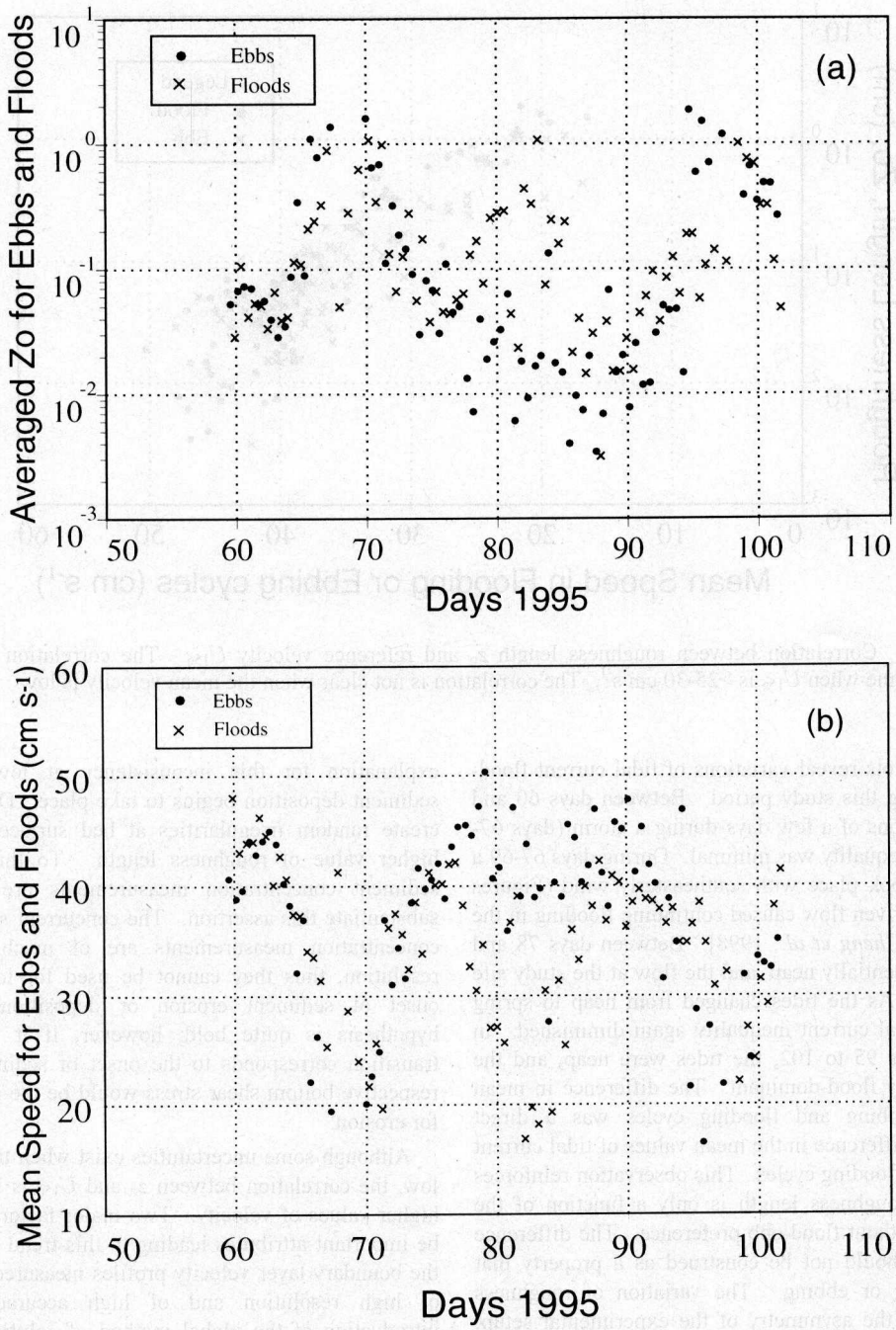

Figure 9. (a) Variations of z_o in 43 days. The z_o values were computed by the global method for each ebbing cycles (solid circles) and for each flooding cycle (crosses). (b) The mean reference velocity U_{156} for each ebbing (solid circles) and for each flooding cycle (crosses).

flooding (crosses) cycles are shown in Figure 9b. There is a pattern of spring-neap variation but not a clear pattern consistent with flooding or ebbing of tidal currents. On closer inspection, regardless of whether the tidal current is flooding or ebbing, the roughness length z_o depends strongly upon mean velocity outside the boundary layer. The variations of z_o in ebbing and flooding cycles are directly correlated to values of mean velocity for the subperiods. Using the mean U_{156} as the reference velocity, the roughness length z_o shows a single correlation with U_{156} (Figure 10), independent of flooding and ebbing cycles. The lack of identifiable properties associated with flooding and ebbing cycles implies that the turbulence at the study site is mostly local production, rather than advected from upstream. The difference in the boundary layer properties (z_o, u_*, and C_d) is the result of tidal current flood-ebb inequality rather than the orientations of flooding and ebbing.

In San Francisco Bay the tidal current flood-ebb inequality exists and varies in a spring-neap cycle. The reference velocity U_{156} time-series plots are shown in Figure 3b and 3c, and the mean speeds for ebbing and flooding cycles are also shown in

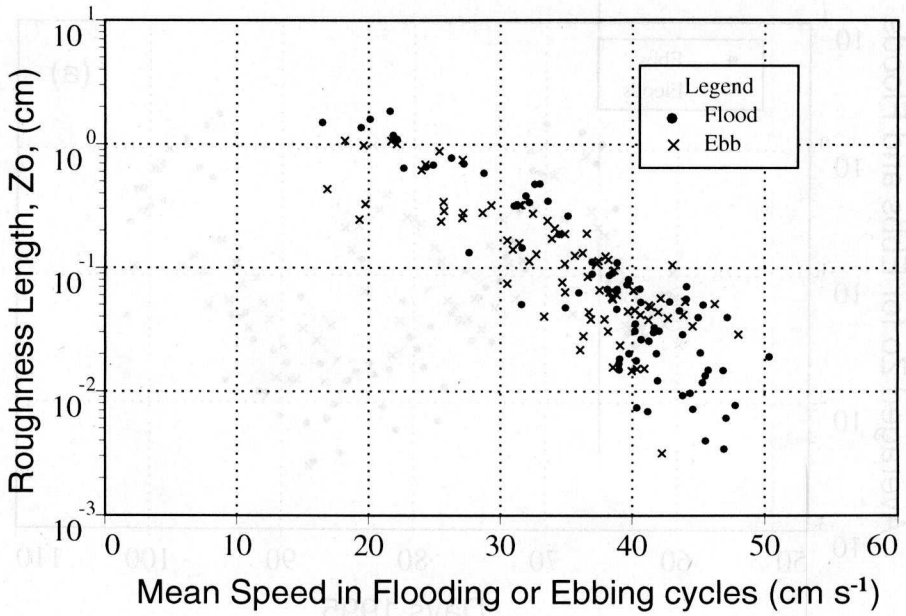

Figure 10. Correlation between roughness length z_o and reference velocity U_{156}. The correlation shows an erosion regime when U_{156} is >25-30 cm s^{-1}. The correlation is not clear when the mean velocity is low.

Figure 9b. These plots reveal variations of tidal current flood-ebb inequality during this study period. Between days 60 and 72, with the exceptions of a few days during a storm (days 67-69), the flood-ebb inequality was minimal. During days 67-69 a major storm event took place with southeasterly wind (Figures 3d and 3e). Wind-driven flow caused continuing flooding in the channel for 2 days [*Cheng et al.*, 1998]. Between days 78 and 85 the tides were essentially neap, and the flow at the study site was ebb-dominant. As the tides changed from neap to spring (days 85-95), the tidal current inequality again diminished. In the next period, days 95 to 102, the tides were neap, and the currents were slightly flood-dominant. The difference in mean values of z_o for ebbing and flooding cycles was a direct consequence of the difference in the mean values of tidal current speed in ebbing and flooding cycles. This observation reinforces the claim that the roughness length is only a function of the reference velocity without flood-ebb preference. The difference in mean z_o values should not be construed as a property that depends on flooding or ebbing. The variation of roughness length is not due to the asymmetry of the experimental setup; instead, the roughness length is shown to be related to tidal current inequality.

3.7. Critical Shear Stress for Erosion

The correlation between the roughness length and the reference velocity is very revealing and interesting. When the reference velocity is >25-30 cm s^{-1}, the logarithmic roughness length ln z_o decreases approximately linearly with increasing reference velocity. Because there is no distinguishable pattern in z_o values due to flooding and ebbing, it is plausible to hypothesize that when the reference velocity is >25-30 cm s^{-1}, the bed form begins to erode (onset of erosion). Higher free-stream velocity results in more effective erosion and a reduction in form drag at the sediment-water interface and hence smaller values of z_o. When the reference velocity is <25-30 cm s^{-1}, the z_o and U_{156} correlation is less consistent. One possible explanation for this inconsistency at low velocity is that sediment deposition begins to take place. Deposited sediments create random irregularities at bed surface, which lead to a higher value of roughness length. To this end the present sediment concentration measurements are not sufficient to substantiate this assertion. The concurrent suspended sediment concentration measurements are of much less quality and resolution, thus they cannot be used for identification of the onset of sediment erosion or deposition. The proposed hypothesis is quite bold; however, if it is valid, then the transition corresponds to the onset of sediment erosion. The respective bottom shear stress would be the critical shear stress for erosion.

Although some uncertainties exist when the mean velocity is low, the correlation between z_o and U_{156} is less certain than at higher values of velocity. Two major factors are considered to be important attributes leading to this trend and pattern. First, the boundary layer velocity profiles measured by BB-ADCP are of high resolution and of high accuracy. Second, the introduction of the global method of solution for deducing z_o provides more accurate and reliable z_o values. Unfortunately, the quality of sediment data is not sufficient to state with certainty that this trend of decreasing z_o with increasing velocity is caused by sediment erosion. However, this mechanism appears to be reasonable and plausible. If one accepts this assumption, then when the mean velocity approaches a certain low value, it should correspond to a stable regime when suspended sediments begin to settle. The bed form would be modified by sediment deposition. The velocity corresponding to the transition between erosion and stable regimes identifies the onset of sediment erosion, which can be used to estimate critical shear stress for erosion. The critical shear stress is one of the key factors in studies of sediment transport. Unfortunately, the critical shear stress is extremely difficult to obtain; there is no previous direct measurement of critical shear stress in San Francisco Bay that might illuminate this situation. Although

the present data set is inadequate to resolve this issue, it does point out an important area of research that could potentially provide insights into critical shear stress for erosion.

4. Summary and Discussions

Insufficient knowledge of hydrodynamic characteristics in BBL is a major weakness in the present understanding of vertical mixing and particulate transport. A field investigation of hydrodynamics and resuspension and transport of particulate matter in a BBL was carried out in South San Francisco Bay, California, during March-April 1995. This field investigation shows that BB-ADCP can be used to measure detailed and accurate time-series of velocity profiles within the turbulent bottom boundary layer in estuaries. The field experiment was designed to keep the physical setting as simple as possible so that the BBL was driven only by barotropic tidal currents without the influences of surface wind-waves nor density stratification. Applications of BB-ADCP for boundary layer flow measurements are unique; high vertical resolution in measured velocity profiles leads to lower errors in deduced friction velocity and bottom roughness length. The only limitation is that some velocity measurements are lost owing to decorrelation of echoes in the high-resolution mode of BB-ADCP. The magnitude of velocity near bed is commonly low. Despite this hardware limitation, valuable and insightful hydrodynamic boundary layer data have been obtained in this field investigation.

The time series of velocity profiles measured by the BB-ADCP has been validated by independent measurements and regarded as high quality. These velocity profiles can be used to test hypotheses of BBL theories. In this paper, for the purpose of deducing u_* and z_o, the velocity distribution in the boundary layer is assumed to be a fully rough turbulent boundary layer, and the velocity distribution is prescribed by the law of the wall. The effects of flow acceleration or deceleration are not considered. The initial data analysis excludes these velocity profiles, which do not qualify as logarithmic profiles. If acceleration and deceleration are considered, a pressure gradient would be present in the direction of flow that would give a higher slope to the law of the wall in (1) [*Soulsby and Dyer*, 1981; *Soulsby*, 1983] and therefore slightly different values of z_o. After u_* and z_o have been computed (excluding those velocity profiles that do not fit the law of the wall with $R^2 < 0.8$) the Reynolds number based on u_* is typically of the order of several hundreds. This confirms that the boundary layer is indeed fully rough.

Three methods for deducing total roughness length are considered. The conventional method of fitting velocity profiles to the law of the wall gives highly scattered z_o values. A global method of solution assumes that the bed resistance remains unchanged for a short period. A group of velocity profiles sharing a mean roughness length is fitted to the law of the wall simultaneously. An error analysis shows that the global method gives more consistent values of friction velocity u_* and roughness length z_o. A simple log-averaged method has been shown to be a good approximation to the global method of solution. The roughness length has been shown to correlate well with a reference velocity independent of flooding or ebbing orientations. Any difference in boundary layer properties in ebbing and flooding cycles is solely due to tidal current flood-ebb inequality and is not caused by the asymmetry of the experimental setup. Thus the turbulence at the study site is mostly local production and is not advected from upstream. A drag coefficient can be introduced which is the slope of correlation between the bottom shear stress u_*^2 and a reference velocity U_{156}^2. The field data presented in this paper show that the roughness length varies with the spring-neap tidal cycle. Thus the drag coefficient cannot remain constant as the drag coefficient is also a function of bed roughness length. It varies with the spring-neap tidal cycle as well.

The correlation between ln z_o and the reference velocity U_{156} shows two distinct regimes: namely, a stable regime and an erosion regime. When the reference velocity is <25-30 cm s^{-1}, z_o is more scattered without a definitive pattern. At higher velocity, ln z_o decreases linearly with increasing reference velocity. This correlation suggests that while erosion is taking place, surficial fine sediments are resuspended by higher, more energetic tidal currents. The bottom shear stress at transition between stable and erosion regimes can be interpreted as the critical shear stress for erosion. However, the measured sediment data are insufficient to support these claims.

The validation of velocity measurements made by a BB-ADCP provides a new and powerful technique in support of BBL research. Some insightful BBL properties of San Francisco Bay could not have been obtained without the high-resolution and accurate velocity profile time series and the use of the global method for data analysis.

Acknowledgments. The authors would like to thank reviewer #1 for his/her detailed review and discussions of the original manuscript.

References

Barenblatt, G. I., Scaling laws for fully developed turbulent shear flows, 1, Basic hypothesis and analysis, *J. Fluid Mech., 248,* 513-520, 1993a.

Barenblatt, G. I., Scaling laws for fully developed turbulent shear flows, 2, Processing of experimental data flows, *J. Fluid Mech., 248,* 521-529, 1993b.

Cacchione, D. A., and D. E. Drake, A new instrument system to investigate sediment dynamics on continental shelf, *Mar. Geol., 30,* 299-312, 1979.

Cacchione, D. A., D. E. Drake, R. W. Kayen, R. W. Sternberg, G. C. Kineke, and G. B. Tate, Measurements in the bottom boundary layer on the Amazon subaqueous delta, *Mar. Geol., 125,* 235-257, 1995.

Cheng, R. T., J. W. Gartner, and R. E. Smith, Bottom boundary layer in South San Francisco Bay, California, *J. Coastal Research, SI 25,* 49-62, 1997.

Cheng, R. T., D. A. Cacchione, J. W. Gartner, and G. B. Tate, Flow and suspended particulate transport in a tidal bottom layer, South San Francisco Bay, California, in *Physics of Estuaries and Coastal Seas,* edited by J. Dronkers and M. B. A. M. Scheffers, pp. 3-12, Balkema, Rotterdam, Netherlands, 1998.

Drake, D. E., and D. A. Cacchione, Field observations of bed shear stress and sediment resuspension on continental shelves, Alaska and California, *Cont. Shelf Res., 6,* 415-429, 1986.

Gartner, J. W., and R. T. Cheng, Near bottom velocity measurements in San Francisco Bay, California, *IEEE Proceedings,* paper presented at Oceans '96, Mar. Technol. Soc., Fort Lauderdale, Fla, 1996.

Gordon, R. L., *Acoustic Doppler Current Profiler, Principles of Operation: A Practical Primer,* 54 pp., RD Instruments, San Diego, Calif., 1996.

Grant, W. D., and O. S. Madsen, The continental-shelf bottom boundary layer, *Ann. Rev. Fluid Mech., 18,* 265-305, 1986.

Grant, W. D., A. J. Williams III, and S. M. Glenn, Bottom stress estimates and their predication on the northern California continental shelf during CODE-1: The importance of wave-current interaction, *J. Phys. Oceanogr., 14,* 506-527, 1984.

Gross, T. F., and A. R. M. Nowell, Mean flow and turbulence scaling in a tidal boundary layer, *Con. Shelf Res., 2,* 109-126, 1983.

Izumi, Y., Kansas 1968 field program data report, *Environ. Res. Pap. 379,* U. S. Air Force Cam. Res. Lab., Cambridge, Mass., 1971.

Kranck, K., and T. G. Milligan, Characteristics of suspended particles at an 11-hour anchor station in San Francisco Bay, California, *J. Geophys. Res., 97*, 11,373-11,382, 1992.

Lhermitte, R., and U. Lemmin, Open-channel flow and turbulence measurement by high-resolution Doppler sonar, *J. Atmos. and Oceanic Technol., 11*, 1295-1308, 1994.

Ling, C. H., On the calculation of surface shear stress using the profile method, *J. Geophys. Res., 81*, 2581-2582, 1976.

Ling, C. H., and N. Untersteiner, On the calculation of the roughness parameter of sea ice, *J. Geophys. Res., 79*, 4112-4114, 1974.

Lohrmann, A., B. Hackett, and L. P. Roed, High resolution measurements of turbulence, velocity and stress using a pulse-to-pulse coherent sonar, *J. Atmos. Oceanic Technol., 7*, 19-37, 1990.

Nichols, F. H., and J. K. Thompson, Time scales of change in the San Francisco Bay benthos, *Hydrobiologia, 129*, 121-138, 1995.

Schauer, U., Determination of bottom boundary layer parameters at two shallow sea sites using the profile method, *Cont. Shelf Res., 7*, 1211-1230, 1987.

Schlichting, H., *Boundary Layer Theory*, 6th ed., 744 pp., McGraw-Hill, New York, 1962.

Schoellhamer, D. H., Factors affecting suspended-solid concentrations in South San Francisco Bay, California, *J. Geophys. Res., 101*, 12,087-12,095, 1996.

Soulsby, R. L., The bottom boundary layer of shelf seas, in *Physical Oceanography of Coastal and Shelf Seas*, edited by R. Johns, pp. 189-266, Elsevier, New York, 1983.

Soulsby, R. L., and K. R. Dyer, The form of the near-bed velocity profile in a tidally accelerating flow, *J. Geophys. Res., 86*, 8067-8074, 1981.

Sternberg, R. W., D. A. Cacchione, D. E. Drake, and K. Kranck, Suspended sediment transport in an estuarial tidal channel within San Francisco Bay, California, *Mar. Geol., 71*, 237-258, 1986.

Walters, R. A., R. T. Cheng, and T. J. Conomos, Time scales of circulation and mixing processes of San Francisco Bay waters, *Hydrobiologia, 129*, 13-36, 1985.

Xu, J. P., and L. D. Wright, Tests of bed roughness models using field data from the middle Atlantic bight, *Cont. Shelf Res., 15*, 1409-1434, 1995.

Yalin, M. S., *Mechanics of Sediment Transport*, 2nd ed., 298 pp., Pergamon Tarrytown, N. Y., 1977.

R. T. Cheng, J. W. Gartner, and C. H. Ling, U.S. Geological Survey, Water Resources Division, 345 Middlefield Road, M/S 496, Menlo Park, CA, 94025. (rtcheng@usgs.gov)

P. F Wang, Marine Environmental Quality Branch, Space and Naval Warfare Systems Center, 53475 Strothe Road, San Diego, CA, 92152.

(Received November 24, 1997; revised August 29, 1998;
accepted November 2, 1998.)